Optical volume and mass measurements show that mammalian cells swell during mitosis

Ewa Zlotek-Zlotkiewicz,[1]* Sylvain Monnier,[1,2]* Giovanni Cappello,[2] Mael Le Berre,[1]** and Matthieu Piel[1]**

[1]UMR 144 and [2]UMR 168, Institut Curie, Centre de Recherche, 75005 Paris, France

The extent, mechanism, and function of cell volume changes during specific cellular events, such as cell migration and cell division, have been poorly studied, mostly because of a lack of adequate techniques. Here we unambiguously report that a large range of mammalian cell types display a significant increase in volume during mitosis (up to 30%). We further show that this increase in volume is tightly linked to the mitotic state of the cell and not to its spread or rounded shape and is independent of the presence of an intact actomyosin cortex. Importantly, this volume increase is not accompanied by an increase in dry mass and thus corresponds to a decrease in cell density. This mitotic swelling might have important consequences for mitotic progression: it might contribute to produce strong pushing forces, allowing mitotic cells to round up; it might also, by lowering cytoplasmic density, contribute to the large change of physicochemical properties observed in mitotic cells.

Introduction

As cells enter mitosis, they dramatically change their shape and round up (Lancaster and Baum, 2014). This change is driven by translocation of the cdk1 substrate Ect2 from the nucleus to the cytoplasm coupled to a loss of adhesion and to actomyosin cytoskeleton remodeling (Matthews et al., 2012). Mitotic rounding has recently been shown to be associated with transient pressure increase providing force to push on the cell surroundings (Stewart et al., 2011). Evidences demonstrate that rounding is crucial to achieve robust chromosomal segregation and so is vital for normal cell division (Lancaster et al., 2013; Cadart et al., 2014). This rapid change of shape might therefore be important not only for tissue morphogenesis (Kondo and Hayashi, 2013) and homeostasis (Nakajima et al., 2013) but also during cancer progression, because tumor growth generates high solid stress (Stylianopoulos et al., 2012), which can induce mitotic arrest (Desmaison et al., 2013). We and others have hypothesized (Cadart et al., 2014) that mitotic cell rounding might be driven, at least under confinement, by an osmotic swelling, a phenomenon that can produce very large forces and is crucial for the growth of walled cells such as plants and fungi but has not been evidenced yet in mammalian cells. If this hypothesis was true, mitotic cells should increase their volume during mitosis. This important point has been debated so far in the literature.

Accurate volume measurements during mitosis of adherent cells are particularly demanding, as cells undergo, both in culture and in tissues, important changes in shape. So far, volume measurements have produced a limited number of results (Habela and Sontheimer, 2007; Boucrot and Kirchhausen, 2008; Huang et al., 2012; Fischer-Friedrich et al., 2014) and led to contradictory conclusions. Data from confocal reconstructions showed a volume decrease at mitotic entry for adherent cells (Habela and Sontheimer, 2007; Boucrot and Kirchhausen, 2008), whereas atomic force microscopy measurements of nonadherent cell height combined with confocal microscopy showed a volume increase (Fischer-Friedrich et al., 2014). For spread cells with complex shapes, volume calculation from 3D reconstruction of the cell boundary could lead to large errors. Even for spherical cells in suspension (Tzur et al., 2009), a very good estimate of cell diameter is needed, as volume depends on the cube of this measure; a 10% increase of volume of a sphere of 8-µm radius results in an increase of radius of only 0.25 µm. Lastly, impedance-based Coulter counter volume measurements are precise but limited to populations of cells in suspension and do not allow temporal tracking of individual cells (Gregg and Steidley, 1965; Tzur et al., 2009; Bryan et al., 2012). As a consequence, there is no consensus on cell volume changes during mitosis. Grover et al. (2011) introduced a new method to measure single-cell volume and density using the suspended microchannel resonator. In this issue, Son et al. advanced the method to enable dynamic measurements and showed that suspended lymphocytic leukemia and pro-B-cell lymphoid cells transiently increase their volume by more than 10% in mitosis.

To measure cell volume of single cells for several hours, we adapted the fluorescence exclusion method (FXm) first proposed

*E. Zlotek-Zlotkiewicz and S. Monnier contributed equally to this paper.

**M. Le Berre and M. Piel contributed equally to this paper.

Correspondence to Mael Le Beurre: mael.leberre@curie.fr; or Matthieu Piel: matthieu.piel@curie.fr

Abbreviations used in this paper: FXm, fluorescence exclusion method; GUVs, giant unilamellar vesicles; PDMS, poly(dimethylsiloxane); RI, refractive index.

The Rockefeller University Press $30.00
J. Cell Biol. Vol. 211 No. 4 765–774
www.jcb.org/cgi/doi/10.1083/jcb.201505056

by Gray et al. (1983) and more recently used by Verkhovsky and co-workers for migrating cells (Bottier et al., 2011; Gabella et al., 2014). We recorded single-cell volume during mitosis for a broad range of cell lines (from adherent cells to cells in suspension). We unambiguously observed a transient and significant cell volume increase during cell division that could reach up to 30% for certain cells. Using quantitative phase microscopy, we demonstrate that the dry mass is constant during mitosis, which results in a cell density drop, and that an intact actomyosin cortex is not necessary to regulate this process. This suggests that mitotic volume increase relies more directly on a transient activation of some ion pumps, which remain to be precisely identified.

Results and discussion

FXm

Cells were grown in poly(dimethylsiloxane) (PDMS) chambers with a ceiling of constant and well-defined height (see Materials and methods). Fluorescent dextran, a hydrophilic polysaccharide that does not cross the cell membrane, was added to the cell culture medium. In such conditions, cells and other objects that exclude the dye appeared as areas of lower fluorescence intensity (Fig. 1 A and Fig. S1, A–C). The height of the chamber was adjusted according to the size of the cells to optimize the signal to noise ratio of the imaging ($h \in [15{:}25]$ µm depending on the cell type). As the height of the chamber is constant, the drop in fluorescence at a given pixel and time point ($\Delta I(x, y, t)$) is proportional to the height of the object (h): $\Delta I(x, y, t) = \alpha \times h(x, y, t)$ (see Materials and methods and Fig. S1, D and E). Calibration was performed for each field of view and every time point by extracting the coefficient α using the value of fluorescence for the central region of the supporting pillars bound to the coverslip (see Materials and methods and Fig. S1, D and E). Cell volume was finally obtained by integrating the fluorescence intensity drop over all the pixels occupied by the cell (Fig. 1 A and Fig. S1 I; see Materials and methods). With this method, a single image with a low-magnification objective enabled us to extract the volume of a large number of individual cells.

We characterized the precision of our method using giant unilamellar vesicles (GUVs; see Materials and methods) of a perfect spherical shape. We measured the radius of GUVs made with rhodamin-conjugated lipids to calculate their volume and compare it to our FXm measurement (Fig. S1 F). The volumes calculated with FXm were in very good agreement with volumes derived from GUV diameter. Based on this comparison, the precision of the absolute volume assessment was high, exhibiting an error between 10% and 14% depending on the objective used (see Materials and methods and Fig. S1 H). The error for the absolute volume is, however, largely overestimated, as it includes the error for GUV diameter measurement. The relative precision is much lower (1%), as it only includes local variations (see Materials and methods). The method is thus well suited to measure temporal variations in volume. As FXm relies on integration of the fluorescent signal over the whole height of the chamber, it is preferable to use objectives with low numerical aperture to conduct measurements in chambers several micrometers deep. We calculated the volume of GUVs by FXm and by measuring their diameter using different objectives to ensure that our volume measurement remained accurate even for 20× objectives with numerical apertures up to 0.75 (Fig. S1 G). Nevertheless, for such objectives, the volume measured by FXm depended more on the accuracy of the focal plane choice. For low-aperture objectives, FXm measurements were completely insensitive to very large variations in focusing, bringing further robustness to the method for long-term imaging of live, moving, and changing-shape cells (Fig. S1 G).

Chamber height was adapted so that during mitosis, at maximal cell height, cells would not touch the chamber ceiling, preventing any mechanical perturbation. To ensure that proper growth conditions were met, we checked that the duration of mitosis and of the entire cell division cycle was similar inside and outside of the volume measurement chambers for HeLa cells (Fig. S2, A and B). To further confirm that cell growth was not perturbed inside chambers, we measured the distributions of cell size at birth and before division for three different cell types and observed that cell size was doubling during one cell division cycle (Fig. S2 C).

Cells increase their volume during mitosis

We recorded the volume of proliferating HeLa cells and observed that individual cell volume grew in a complex nonlinear manner to roughly double before the next mitosis. Instead of plateauing, cell volume displayed a sharp increase at mitotic onset (20.7 ± 0.7%, $n = 60$; Fig. 1, B and C). This was followed by a volume loss at mitotic exit, so that the summed volume of the two daughter cells at birth corresponded to the volume of their mother at mitotic entry (Fig. 1 C). To further study this transient mitotic volume increase, we monitored HeLa cells expressing histone H2B-mCherry (Fig. 1 D) and performed faster time-lapse recordings throughout mitosis. Cell volume increased concomitantly with cell rounding, reached a maximum during metaphase, and started to decrease shortly before anaphase (Fig. 1, D and E). This observation proved to be robust when averaged over many single cells (Fig. 1, F–H), showing that mitotic entry was accompanied by a sharp volume increase and mitotic exit by an equivalent loss of volume. We call this transient increase in volume "mitotic swelling."

Mitotic swelling is independent of cell adhesion or change in cell shape

Because mitotic entry and exit correspond, in HeLa cells, to a drastic change of cell shape, we asked whether the increase in volume was caused by the change in shape or to the mitotic state of the cell. First, HeLa cells expressing histone H2B-mCherry were placed in chambers coated with PLL-g-PEG to prevent cell adhesion. In these conditions, cells were already rounded before mitotic entry. We detected mitotic entry using the fluorescently labeled histones (Fig. 2 A). These prerounded cells showed the same transient mitotic volume increase (17.5% ± 0.8%, $n = 14$) as flat and adherent HeLa cells (20.7 ± 0.7%, $n = 60$; Fig. 2, B and C). We then induced rounding of interphase HeLa cells using PBS-EDTA treatment. The volume of interphase cells remained constant before and after this induced rounding (1.2% ± 1.2%, $n = 21$; Fig. 2, D–F). This shows that neither the change of shape itself nor the loss of adhesion alone affected cell volume or our measurements. Collectively, these results show that there is a fast and transient volume increase tightly linked to the mitotic state of the cell and independent of its shape. Using multiple drugs to perturb mitosis, Son et al. (2015) confirmed the strong link between volume change of the cell and its mitotic state.

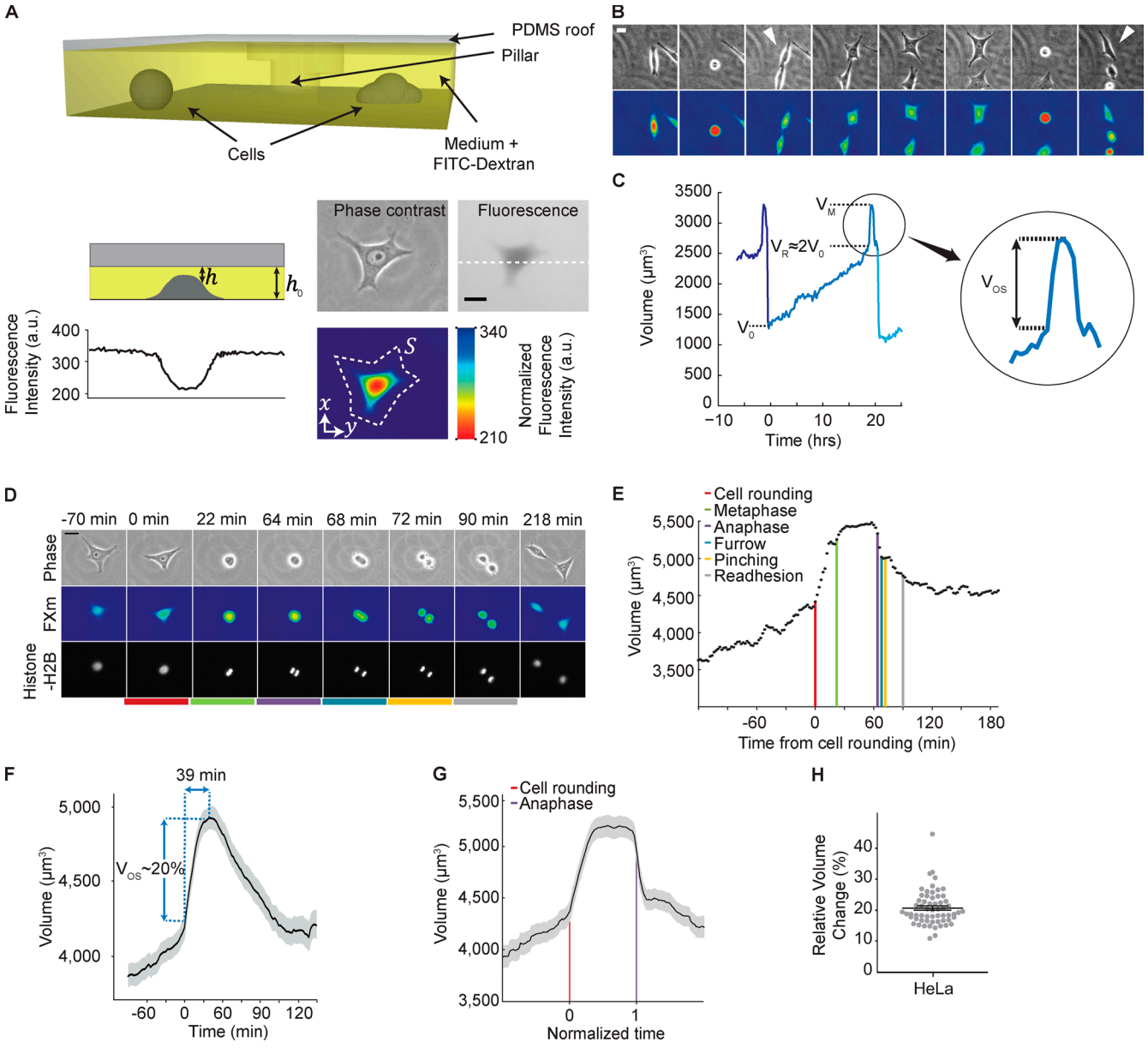

Figure 1. **Cell volume increases transiently during mitosis.** (A) Sketch of the thin PDMS chamber filled with fluorescent dextran for volume measurements, cross section of the chamber with the corresponding profile of fluorescence, and images of a cell in phase contrast and fluorescence in gray levels and false colors. Dashed lines on the grayscale image correspond to the sketch and profile on the left and on the color scale image show the integration area for calculation of cell volume. (B) Time-lapse images of HeLa cells in phase contrast and FXm. Arrows correspond to cells whose volume is shown in C. (C) Whole cell cycle volume trajectory, where arrows correspond to cells shown in B. V_0, cell volume at birth; V_R, volume at rounding; and V_M, maximum volume reached during mitotic swelling. Close-up shows the volume overshoot occurring during mitosis ($V_{OS} = V_M - V_R$). (D) Time-lapse images of a HeLa cell stably expressing histone H2B-mCherry, in phase contrast, with FXm and in fluorescence for mCherry (Video 1). (E) Absolute volume as a function of time for the HeLa cell and the two daughters shown in D, with a time lapse every 2 min. Colored lines indicate successive mitotic events. (F) Mean volume overshoot for $n = 25$ mitotic HeLa cells in one single experiment. Time registered at cell mitotic rounding (time = 0), and SEM is shown in gray. (G) Mean volume as in F, with time registered at cell mitotic rounding (time = 0) and normalized for mitosis length (anaphase at time = 1). Mean overshoot is 21.02%, and SEM is shown in gray. (H) Relative volume change in mitosis (V_{OS} = 20.72%, SEM = 0.73, $n = 60$, $N = 2$). Bars, 20 µm.

Mitotic swelling can be detected based on measurement of the cell diameter

To check if the mitotic volume overshoot could be seen by measuring cell diameter, we imaged rounded HeLa Life-Act-mCherry cells cultured in nonadhesive chambers (Fig. 2 G). Fitting the perimeter of cells to extract their radius and calculate their volume showed that this method was sufficient to measure a volume increase during mitosis and provided the same estimate for the mean volume increase, but with much more variability in the measures compared with FXm (Fig. 2 G). We also reproduced the geometry studied in Fischer-Friedrich et al. (2014) by confining cells between two surfaces (Lancaster et al., 2013; Le Berre et al., 2014). In this geometry, cell height was constant and only the surface area changed with the volume. Similarly, we observed a significant increase of cell surface in mitosis (Fig. 2 H). Blebs were not taken into account in these measures, and this could explain the smaller volume increase obtained in this configuration.

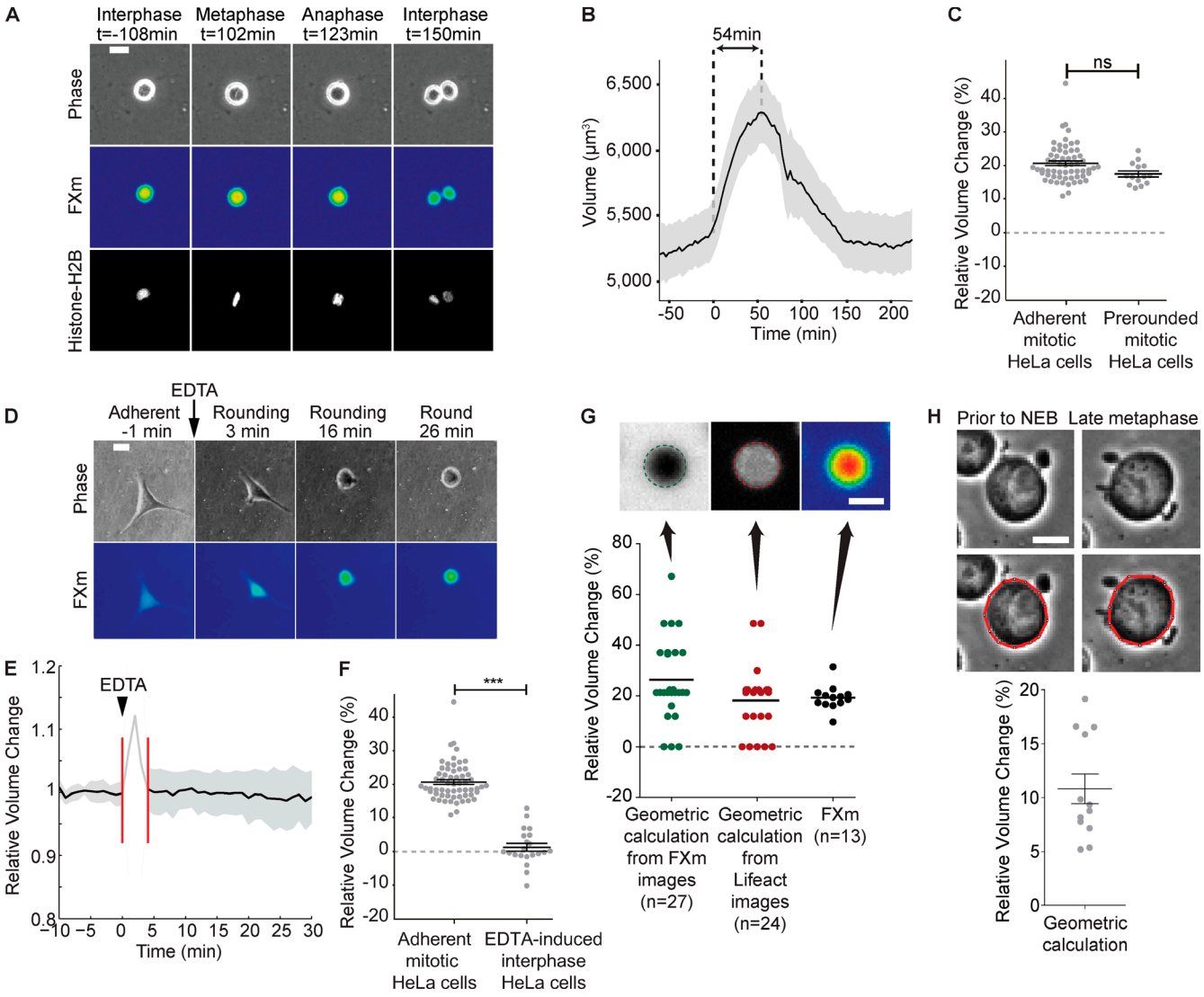

Figure 2. **Mitotic swelling is independent of cell shape, adhesion, or geometry.** (A) Time-lapse images of a prerounded cell before entering mitosis (−108 min) and at metaphase, anaphase, and after cell division (150 min; phase contrast, FXm, H2B-mCherry; Video 2). (B) Mean volume of H2B-mCherry expressing HeLa cells ongoing division in conditions to prevent cell adhesion (n = 14, N = 3, overshoot = 17.49%, SEM is shown in gray). (C) Volume change for adherent cells entering mitosis (same as Fig. 1 H) and for prerounded cells entering mitosis (n = 14, N = 3, overshoot = 17.49% [SEM = 0.88]). (D) Time-lapse images of an adherent cell just before adding EDTA, during early detachment, while rounding up, and completely rounded (phase contrast, FXm; Video 3). (E) Mean relative volume change of interphase HeLa cells during EDTA-induced detachment and rounding (volume before EDTA injection is normalized to 1; see Materials and methods and Video 3; n = 21, N = 2, ΔV = 1.27%, SEM is shown in gray). (F) Volume change for adherent HeLa cells entering mitosis (same as Fig. 1 H) and for detaching interphase cells after EDTA treatment (n = 21, N = 2, ΔV = 1.27% [SEM = 1.15]; ***, $P < 0.0001$). (G) Mitotic volume overshoot for prerounded HeLa cells cultured in PLL-g-PEG–coated chambers. Volume calculations were done by fitting the maximal diameter with a circle from FXm and Lifeact images at mitotic onset and before anaphase and compared with FXm measurements. (H) Volume overshoot of HeLa cells confined between two plates. Volume is obtained by fitting the periphery of the cell before nuclear envelope breakdown and at late metaphase. Bars, 20 µm.

Swelling is independent of the actomyosin cytoskeleton

The actomyosin cortex plays an important role in mitotic cell shape and was previously proposed to counteract osmotic forces during mitotic rounding (Stewart et al., 2011). We thus tested if perturbing the cortex had an effect on volume increase during mitosis. We used drugs to destabilize filamentous actin (latrunculin A) or impede myosin II activity (Y-27632). We used HeLa cells expressing LifeAct-mCherry to monitor the effect of latrunculin A treatment and could completely remove the actin cortex of mitotic cells inside the chambers used for FXm during the whole duration of the experiment (Fig. 3 A, top; note that a high dose of latrunculin A [5 µM] was required, probably because of long-term titration of this hydrophobic drug by the PDMS walls of the chamber). Similarly, HeLa cells expressing MYH9-GFP (myosin II A heavy chain) were used to check that treatment with Y27632 completely removed the cortical myosin II staining (Fig. 3 A, bottom). Neither complete removal of the actin cortex nor inhibition of myosin II activity significantly affected the mitotic swelling (Fig. 3 B; note that because treated cells tend to round up, we included a control with cells cultured on PLL-PEG substrate and thus having a round shape before mitosis). Together, these results show that, at least for HeLa cells, mitotic swelling does not depend upon and is not regulated by the actomyosin cortex.

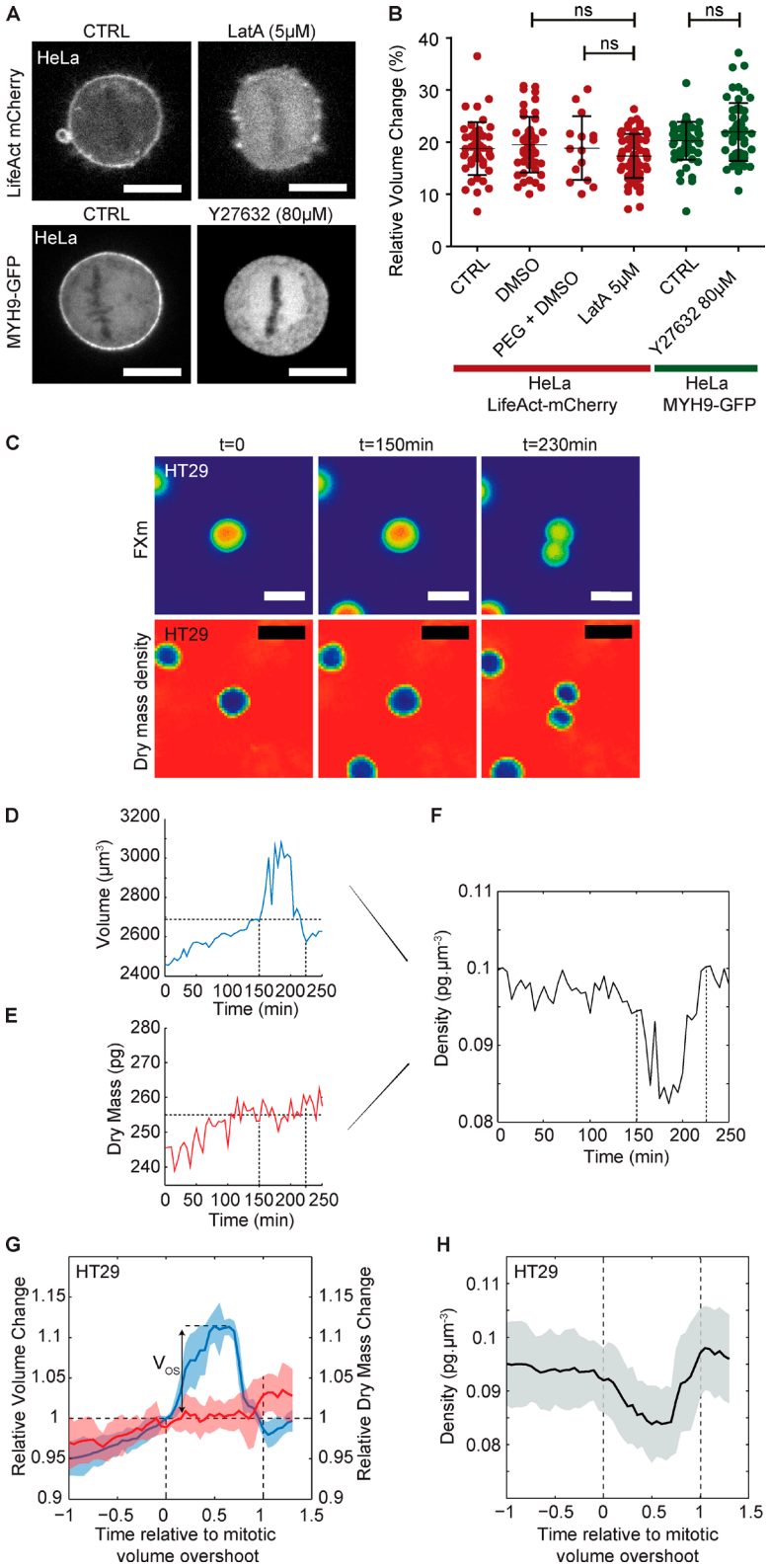

Figure 3. **Mitotic swelling is independent of actin cortex integrity and contractility and is accompanied by a drop in cell density.** (A) Images of LifeAct-mCherry HeLa cells treated with 5 µM latrunculin A and MYH9-GFP HeLa cells treated with 80 µM ROCK inhibitor Y27632. Bars, 20 µm. (B) Relative mitotic volume change for HeLa cells treated with latrunculin A (red) and Y27632 (green), with three types of controls: untreated cells (CRTL), addition of DMSO only, and cells in nonadherent chambers with DMSO. (C) Images of an HT29 cell undergoing mitosis with FXm and dry mass density imaging. Bars: (top) 20 µm; (bottom) 24 µm. (D and E) Volume and dry mass for the cell in C. (F) Density of the cell in C calculated from the volume and dry mass. (G) Mean volume and dry mass in mitosis for HT29 cells. Volume and mass are normalized to 1 and time is set to 0 at volume overshoot start, and time is set to 1 at the end of the overshoot (D–F, dashed line). Light blue and red areas show the SD for volume and mass, respectively (n = 8 for G). (H) Mean cell density for HT29 cells, where time is set to 0 and 1 at volume overshoot start and end, respectively. The SD is shown as the gray area.

Mitotic swelling is associated with a decrease in cell density

To assess if mitotic swelling was caused by increasing cell mass, we simultaneously measured the volume and the dry mass of single HT29 cells using quantitative phase microscopy (Bon et al., 2009; Zangle and Teitell, 2014) combined with FXm (Fig. 3 C; see Materials and methods). The obtained density is the ratio between cell dry mass and volume and is different from the density measured by Son et al. (2015) in this issue, as the latter is based on the total cell mass. Our measurements showed that although cell volume increased (Fig. 3 D), dry mass was constant during mitosis (Fig. 3 E), resulting in a drop of cell density (Fig. 3, F and H). This observation was confirmed using HeLa cells (Fig. S2, D–F). Therefore, osmolites that caused

mitotic swelling did not contribute to cell dry mass and were likely small osmolites such as ions. Son et al. (2015) similarly observed a drop in density and further showed that this resulted from water entry and not endocytosis.

Mitotic swelling is observed in a large range of mammalian cells

As other studies have reported a volume decrease during or before mitosis (Habela and Sontheimer, 2007; Boucrot and Kirchhausen, 2008; Huang et al., 2012), we extended our observation to other cell lines. We studied both adherent and nonadherent cells, with different morphologies, derived from different organisms and tissues. All of the cell types we observed showed a significant increase in volume during mitosis, but with different amplitudes (from 10% to over 20%; Fig. 4, A–D). None of the cell lines we assayed (and none of the single cells we measured) showed a decrease in volume during mitosis. Adherent cells (HeLa, V_{OS} = 20.7 ± 0.7%, n = 60; S180, V_{OS} = 22.1 ± 1.3%, n = 19; L929, V_{OS} = 18 ± 0.7%, n = 40) showed a larger volume increase than poorly adhesive rounded (HT29, V_{OS} = 15.4 ± 0.7%, n = 44) or nonadherent cells (Raji, V_{OS} = 11.3 ± 0.4%, n = 67; Fig. 4, A–D). Note that Raji cells can be compared with L-1210 and FL5.12 cells used by Son et al. (2015) and that similar swelling rates were obtained using both methods (Raji 11%, L-1210 12%, and FL5.12 11%). Aside from the variability from one cell line to another, cell lines with larger cell size tend to display larger swelling (P = 0.01; Fig. 4 F), resulting in similar relative volume increase (P = 0.49; Fig. 4 E). Within a given cell line (for HeLa, HT29, and Raji cells), at the single cell level, we did not observe any correlation between volume increase and size of the cell at mitosis onset (Fig. S3, A–D) or the duration of mitosis (Fig. S3 E). This might be caused by smaller spread of sizes within one cell line and the existence of another source of variability masking the tendency observed between different cell lines. Altogether, our data suggest that mitotic swelling is a universal phenomenon for cultured mammalian cells.

In conclusion, most mammalian cells, both in vivo and in vitro, undergo a drastic change of shape at mitosis. This mitotic rounding has been proposed to play an important role in developmental processes and to be involved in morphogenetic events (Kondo and Hayashi, 2013). We have recently proposed that mitotic rounding is important to generate enough space for robust spindle assembly and chromosome segregation (Lancaster et al., 2013; Cadart et al., 2014). It is thus a crucial phenomenon for the fidelity of the mitotic process and thus for the survival of proliferating cells. Mitotic cell rounding is associated with cell cortex reorganization and stiffening (Matthews et al., 2012; Lancaster et al., 2013). It was recently shown that stiffening and increase in contractility associated to mitotic rounding could produce pushing forces (Stewart et al., 2011). In the context of a dense tissue, these pushing forces might be essential to achieve a spherical shape and secure enough space for robust spindle assembly and orientation. These pushing forces were attributed both to the increase in surface tension caused by increased myosin recruitment at the cell cortex (Fischer-Friedrich et al., 2014; Ramanathan et al., 2015) and an osmotic swelling (Stewart et al., 2011). This last aspect is crucial because osmotic swelling can produce very large forces, even with very small changes in osmolarity (10% increase in osmolarity corresponds to 80 kPa for a mammalian cell whose osmolarity is ∼330 mOsm; see Materials and methods). It would also imply that new players, such as ion pumps, are involved, as suggested by Son et al. (2015) using ethylisopropylamiloride, which inhibits Na-H transporters. In the absence of resisting forces, an increase in osmolarity of the cell should very rapidly translate in a corresponding increase in volume.

Precise cell volume measurements are challenging to perform during dynamic changes in cell shape and over long periods of time and were so far performed either with techniques restricted to cells with a simple and constant shape (Tzur et al., 2009) or using 3D surface reconstruction. Here, using a precise and simple technique, we unambiguously demonstrate that all cultured mammalian cell lines that we assayed displayed a significant volume increase during mitosis. In this issue, Son et al. (2015), using a suspended microchannel resonator based on physical measurement of the cells' buoyant mass, observed a similar cell volume increase in mitosis for suspended cells. This volume increase, although hardly measurable by other means, is important enough to produce potentially very large pushing forces if cells were confined.

Our observation that the actin-myosin cortex is neither involved in mitotic swelling nor restrains it could seem surprising, as the cortex has been proposed to counteract internal osmotic pressure (Stewart et al., 2011). However, current measures available for cortical stiffness indicate that surface tension caused by the activity of the actomyosin cytoskeleton could account for changes in cell volume up to only 1% (Salbreux et al., 2012). As recently proposed through physical modeling, the actomyosin cortex could also have a regulatory role through mechanosensitive ion channels (Jiang and Sun, 2013). This does not seem to account for the mitotic swelling in the cell lines we assayed. Accordingly, the most recent measures showed that the actomyosin-dependent rounding pressure came purely from the surface tension (Fischer-Friedrich et al., 2014; Ramanathan et al., 2015). Indeed, in these atomic force microscopy–based experiments, cells were not constrained laterally, and thus any increase in osmolarity exceeding what the surface tension could bear translated in an increase in volume, which was observed (Fischer-Friedrich et al., 2014). On the contrary, in a context in which cells would be constrained in all directions (such as in a dense tissue), an increase in osmolarity could also generate strong pushing forces. According to the volume increase we measured (∼10% or more for most cell lines), the corresponding osmotic pressure (∼100 kPA) could potentially deform almost any tissue (cartilages reach stiffness of the order of 100 kPa; Swift et al., 2013).

Our study thus contributes to clarify a debated point and unambiguously shows that cells transiently increase their volume during mitosis. This increase results in a dilution of the cytoplasm, which might have a strong impact on out-of-equilibrium biochemical processes taking place during cell division. It also suggests that most cells are potentially able to exert strong pushing forces, most likely via activation of ion pumps. Determining which of these pumps could help design new drugs to specifically affect dividing cells embedded in stiff environments such as solid tumors.

Materials and methods

Cell culture

Cells were cultured in appropriate media adapted to each cell line. Media were supplemented with 10% FBS (Life Technologies) and 1% 100× penicillin-streptomycin solution (Life Technologies).

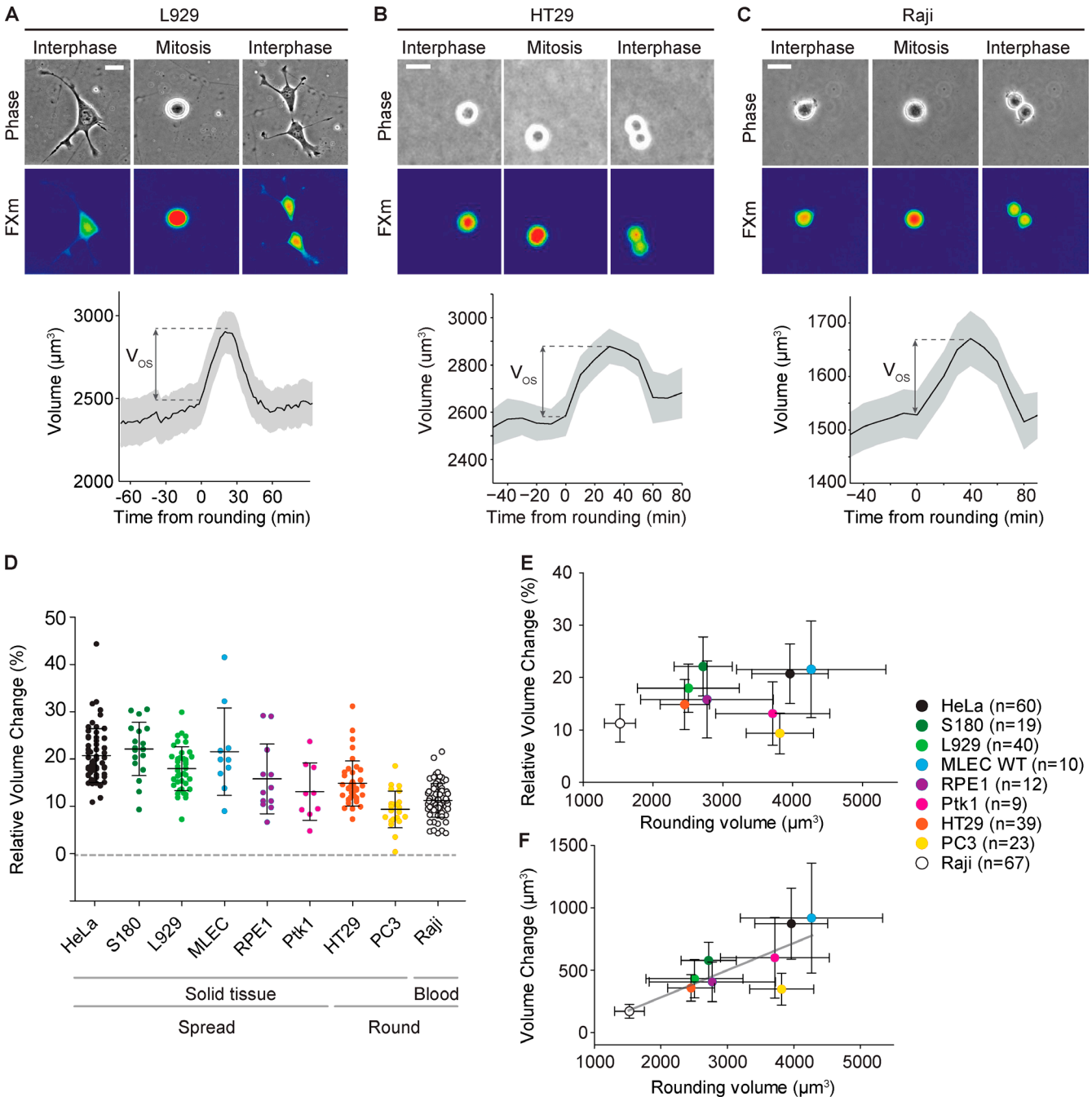

Figure 4. **Mitotic swelling is observed for a large set of cell lines.** (A) Phase and FXm images of a L929 cell, and mean volume of fibroblastic L929 cells undergoing mitosis (n = 38). (B) Phase and FXm images of an adherent HT29 cell, and mean volume of HT29 cells undergoing mitosis (n = 16). (C) Phase and FXm images of a floating Raji cell, and mean volume of Raji cells undergoing mitosis (n = 67). For A–C, time is set to 0 as cells start to round up, and the gray area displays the SEM. (D) Relative increase of volume in mitosis for different cell lines. For each cell, the volume increase is taken between mitotic entry and the maximal volume reached during mitosis. Cells were divided into three categories, from solid tissue with spread or rounded morphology and from blood with a rounded morphology. (E and F) Relative and absolute volume overshoot per cell line as a function of their rounding volume at mitotic entry. The gray line in F shows the linear regression (R^2 = 0.63). Two-tailed t test: P = 0.49 (E) and P = 0.01 (F).

Cell lines

HeLa are cancerous epithelial cells derived from human cervix. S180 and L929 are mouse sarcoma fibroblast cell lines. MLEC are mouse endothelial cells derived from lung. RPE1 and PtK1 are noncancerous epithelial cells derived from human retina pigment and potoroo kidney, respectively. HeLa, S180, L929, MLEC, RPE1, and PtK1 are all adherent cells displaying spread morphologies.

HT29 and PC3 are cancerous human cells derived from colon and prostate, respectively. They grow in adherent culture but exhibit rounded shapes. HT29 cells (HTB-38; ATCC) were provided by D. Vignjevic, Institut Curie, Paris, France. PC3 cells were provided by L. Ghenim-Ziman from the CEA, Grenoble, France.

Raji are human B lymphocyte cells cultured in suspension and have spherical shapes (a gift from C. Hivroz, Institut Curie, Paris, France).

Chip fabrication

Masters were fabricated using a conventional photolithography procedure or micromilling approach. The designs of the brass master molds were created using Catia software (Dassault Systemes). Brass masters were fabricated with a micromilling machine (MiniMill/3; Minitech) using a 100-µm-diameter milling cutter (Minitech). Height profiles and surface roughness were measured with a vertical scanning interferometric profilometer (WYCO NT1100; Veeco). Surface roughness of the brass master and heights variation within one chamber did not exceed 0.2 and 0.3 µm, respectively. The variability in chamber height, set by the height of the pillars, could generate errors on the absolute cell volume up to 2%, a contribution that is already included in the error on the absolute volume (see Volume measurement section).

A 10:1 mixture of PDMS Sylgard 184 or RTV614 silicone elastomer and curing agent was poured onto the brass master and cured at 65°C for 2 h. Inlet and outlet were punched with a 0.75-mm puncher before bonding. Glass-bottomed Petri dishes (homemade or Fluorodish) and PMDS chips were cleaned with isopropanol before a 30-s exposure to oxygen plasma for bonding. Finally, chambers were exposed for 10 min to UV light for sterilization.

Chambers were incubated with 50 µg/ml fibronectin in PBS (Life Technologies) for 1 h for adherent cell types, washed with PBS, and then incubated overnight with medium at room temperature. Chambers were washed with medium before cell insertion. Cells were resuspended in medium supplemented with 1 mg/ml Alexa Fluor 488 Dextran (MW 10 kD; Life Technologies) to a concentration of ∼500,000 cells/ml (depending on the cell type) and then injected in the chamber. Finally, the chamber was immersed in medium to prevent evaporation.

Drug and adhesion experiments

For EDTA-induced cell rounding experiments (Fig. 2, D–F), the medium was first replaced with PBS at least 20 min before adding 1 mM EDTA in PBS. PBS and PBS-EDTA have equal osmolarity. For experiments with prerounded HeLa cells (Fig. 2, A–C), cells were prerounded by placing them in chambers prepared as previously described but coated with PLL-g-PEG (1%) instead of fibronectin after plasma treatment.

Experiments with latrunculin A from Invitrogen and Y27632 from Calbiochem were performed in chambers preincubated with the final concentration of drug one night prior seeding the cells to prevent drug depletion caused by hydrophobicity or PDMS. Images of the cells were taken before launching acquisition to confirm the effect of the drug (Fig. 3 A).

Live-cell imaging

Acquisitions were performed on a Ti inverted (Nikon) or an Axio Observer microscope (Carl Zeiss) at 37°C, with 5% CO_2 atmosphere, using a 10× dry objective (NA 0.30 phase), a 20× dry objective (NA 0.5 phase), or a SFluor 20× objective (NA 0.75 without phase ring) for the mass measurements. Images were acquired using MetaMorph (Molecular Devices) or Axio Vision (Carl Zeiss) software. The excitation source was either a mercury lamp (Intensilight; Nikon) or a LED illumination (SPECTRA X light; Lumencor or Zeiss Colibri). Images were acquired with a CoolSNAP HQ2 camera (Photometrics) for fluorescence or a PHASICS camera (PHASICS) for mass measurements.

GUV measurements and FXm precision

GUVs were used rather than glass beads because the refractive index (RI) of such beads (RI > 1.47) was too different from that of water (RI = 1.33) and thus generated optical artifacts. On the other hand, the refractive index of GUVs was close to that of cells or external media (RI < 1.37; Curl et al., 2005). GUVs were prepared by regular electroformation (Carvalho et al., 2013) with EPC (L-α-phosphatidylcholine) from Sigma-Aldrich, and rhodamin-PE. (1,2-dioleoyl-sn-glycero-3-phosphoethanolamine-N) from Avanti polar lipids was used for membrane labeling. GUVs were placed in hypo-osmotic conditions to ensure their spherical shape, and osmolarity was controlled with a freezing point osmometer (Löser). To prevent vesicle adhesion and deformation, the surface of the chip was blocked with BSA or PLL-g-PEG. Volume measurements were performed at room temperature. Geometrical volume calculations were achieved by fitting the equatorial perimeter with a disk and extracting the radius from the surface of the disk from images of labeled GUVs obtained with a 20× objective. This procedure was performed by the user and not by automatic means. Errors on the geometrical calculations were calculated from a fitting error of the size of one pixel. GUVs with volumes <300 μm^3 were excluded as they generated segmentation defects and would require lower chambers and higher magnification for proper volume calculation. Precision on FXm was obtained for each objectives by calculating the standard deviation for a normal distribution centered on $V_{geom} = V_{FXm}$ (Fig. S1 H). We finally obtained for a 10× with a 0.3 NA SD = 14%, for a 10× NA 0.5 SD = 13%, for a 20 ± NA 0.5 SD = 9.5%, and finally for a 20× objective with a 0.75 NA SD = 10%. These errors include the errors caused by the diameter estimation of the GUVs (likely accounting for most of the error here), the variability on the chamber height, the inhomogeneity of the light illumination, and the image analysis procedure. The relative accuracy (<1%) corresponds to the SD of cell volume over 10 min for a fixed region of interest for cells in PBS.

Volume measurement

Images were analyzed with a custom-made MatLab program (MathWorks). Calibration was performed similarly to Bottier et al. (2011), using the sustaining pillars of multiple heights (Fig. S1, A–E), with the difference that calibration was performed on the same chip where the cells were cultured, and for every field of view and every time point. It gives a linear relationship between the fluorescence intensity and the space filled with the dye: $I = \alpha \times h + I_0$. To extract the coefficient α, calibration using pillars was performed in initial experiments to check for the stability of the method, but was not generally required (Fig. S1, D and E). In general, pillars with a single height were used, and the coefficient was extracted using the region of the supporting pillars bound to the coverslip for I_o and the intensity of the background in the absence of any object, which represents the fluorescence value for the maximal height of the chamber.

Even though a low-magnification objective and LED light source were used, the illumination was never perfectly homogeneous. To extract the background value, cells and pillars were first excluded using an automatic segmentation procedure based on thresholding; the background $I_B(x,y)$ was then fitted with a quadratic polynomial function. Finally, the difference between the background and the image was integrated over the area manually defined by the user corresponding to the cell and divided by α to obtain the cell volume:

$$V_{cell} = \iint_s \frac{I_B(x,y) - I(x,y)}{\alpha} dS.$$

Note that the initial segmentation procedure was used only to exclude cells and pillars to correct for illumination defects. The region used to integrate the cell volume was defined manually and kept constant through time (Fig. S1 I). Importantly, the position of the edges of this region did not matter as long as the region encompassed the whole cell, because the value of the background around the cell after subtraction was zero; the measure was thus completely insensitive to changes in cell shape.

Coupled mass and volume measurements

Mass images were acquired on a PHASICS camera, whereas FXm images were acquired on a regular CoolSNAP HQ2 camera as described in the Live-cell imaging section. For each time point images were acquired with both cameras successively. Later generation of mass images requires acquisition of empty fields; this was performed after time-lapse acquisition by removing the cells with TryPLE. The refraction increment used to calculate dry mass from the optical thickness is $\alpha = 0.180\ \mu m^3.pg^{-1}$ as considered in Barer (1952) and suggested by the company. The dry mass of the cells was calculated as done for the volume by subtracting the background and integrating the mass on the same area used for volume calculation (see above).

Calculation of osmotic force developed at mitosis

We assume that the fast volume change observed at cell rounding is exclusively caused by ion entry generated by active ion pumping, followed by water influx to equilibrate cytoplasm osmolarity with the surrounding medium. Physiological culture medium has typical osmolarity of 330 mOsm. A 10% volume change thus corresponds to the import of 33 mOsm of osmolites. By using the Van't Hoff equation, we can calculate the pressure a cell would be able to generate in a confined environment that would not allow any volume increase: $P = DC \cdot RT$, where R and T are the gas constant and the temperature, respectively. This gives an osmotic pressure of $\Pi \approx 80$ kPA for a 10% increase in cellular volume.

Online supplemental material

Fig. S1 shows calibration of the fluorescence exclusion method (FXm). Fig. S2 shows that the cell division cycle and mitosis durations are not perturbed in the volume measurement chambers and cell density drops in mitosis for HeLa cells. Fig. S3 shows that mitotic swelling is constant for a given cell line. Video 1 shows the whole-cell division cycle for HeLa cells in the FXm chamber, corresponding to the time-lapse images shown in Fig. 1 B. Video 2 shows mitosis of a nonadherent HeLa cell, corresponding to Fig. 2 A. Video 3 shows cell rounding induced by PBS-EDTA, corresponding to Fig. 2 D. Online supplemental material is available at http://www.jcb.org/cgi/content/full/jcb.201505056/DC1.

Acknowledgments

We thank Kévin Carvalho, Joël Lemière, and Fabrice Valentino for the production of GUVs. We thank Jean-François Joanny, Pierre Recho, and Buzz Baum for fruitful discussions; Rémy Fert for micromilling of the chamber molds; and Lamya Ghenim-Ziman for PC3 cells. The authors greatly acknowledge the Nikon Imaging Centre and the PICT-IBI SA plateform at the Institut Curie-Centre National de la Recherche Scientifique.

S. Monnier was supported by the Fondation Pierre-Gilles de Gennes. E. Zlotek-Zlotkiewicz was supported by a PhD fellowship from Institut Multi-Organismes Cancer (Plan Cancer 2009-2013). This work was supported by an Institut National du Cancer grant (PLBIO 11-IC-1) and a European Research Council consolidator grant (PROMICO-311205) to M. Piel.

The authors declare no competing financial interests.

Author contributions: M. Le Berre conceived the cell volume measurement method. S. Monnier, E. Zlotek-Zlotkiewicz, M. Le Berre, G. Cappello, and M. Piel conceived the experiments. S. Monnier and E. Zlotek-Zlotkiewicz performed the experiments and analysis. S. Monnier and M. Le Berre wrote the analysis algorithms. G. Cappello, M. Le Berre, and M. Piel supervised the work. S. Monnier, E. Zlotek-Zlotkiewicz, and M. Piel wrote the paper.

Submitted: 12 May 2015
Accepted: 13 October 2015

References

Barer, R. 1952. Interference microscopy and mass determination. *Nature*. 169:366–367. http://dx.doi.org/10.1038/169366b0

Bon, P., G. Maucort, B. Wattellier, and S. Monneret. 2009. Quadriwave lateral shearing interferometry for quantitative phase microscopy of living cells. *Opt. Express*. 17:13080–13094. http://dx.doi.org/10.1364/OE.17.013080

Bottier, C., C. Gabella, B. Vianay, L. Buscemi, I.F. Sbalzarini, J.-J. Meister, and A.B. Verkhovsky. 2011. Dynamic measurement of the height and volume of migrating cells by a novel fluorescence microscopy technique. *Lab Chip*. 11:3855–3863. http://dx.doi.org/10.1039/c1lc20807a

Boucrot, E., and T. Kirchhausen. 2008. Mammalian cells change volume during mitosis. *PLoS One*. 3:e1477. http://dx.doi.org/10.1371/journal.pone.0001477

Bryan, A.K., A. Engler, A. Gulati, and S.R. Manalis. 2012. Continuous and long-term volume measurements with a commercial Coulter counter. *PLoS One*. 7:e29866. http://dx.doi.org/10.1371/journal.pone.0029866

Cadart, C., E. Zlotek-Zlotkiewicz, M. Le Berre, M. Piel, and H.K. Matthews. 2014. Exploring the function of cell shape and size during mitosis. *Dev. Cell*. 29:159–169. http://dx.doi.org/10.1016/j.devcel.2014.04.009

Carvalho, K., F.C. Tsai, E. Lees, R. Voituriez, G.H. Koenderink, and C. Sykes. 2013. Cell-sized liposomes reveal how actomyosin cortical tension drives shape change. *Proc. Natl. Acad. Sci. USA*. 110:16456–16461. http://dx.doi.org/10.1073/pnas.1221524110

Curl, C.L., C.J. Bellair, T. Harris, B.E. Allman, P.J. Harris, A.G. Stewart, A. Roberts, K.A. Nugent, and L.M. Delbridge. 2005. Refractive index measurement in viable cells using quantitative phase-amplitude microscopy and confocal microscopy. *Cytometry A*. 65:88–92. http://dx.doi.org/10.1002/cyto.a.20134

Desmaison, A., C. Frongia, K. Grenier, B. Ducommun, and V. Loblois. 2013. Mechanical stress impairs mitosis progression in multi- cellular tumor spheroids. *PLoS One*. 8:e80447. http://dx.doi.org/10.1371/journal.pone.0080447

Fischer-Friedrich, E., A.A. Hyman, F. Jülicher, D.J. Müller, and J. Helenius. 2014. Quantification of surface tension and internal pressure generated by single mitotic cells. *Sci. Rep*. 4:6213. http://dx.doi.org/10.1038/srep06213

Gabella, C., E. Bertseva, C. Bottier, N. Piacentini, A. Bornert, S. Jeney, L. Forró, I.F. Sbalzarini, J.-J. Meister, and A.B. Verkhovsky. 2014. Contact angle at the leading edge controls cell protrusion rate. *Curr. Biol*. 24:1126–1132. http://dx.doi.org/10.1016/j.cub.2014.03.050

Gray, M.L., R.A. Hoffman, and W.P. Hansen. 1983. A new method for cell volume measurement based on volume exclusion of a fluorescent dye. *Cytometry*. 3:428–434. http://dx.doi.org/10.1002/cyto.990030607

Gregg, E.C., and K.D. Steidley. 1965. Electrical counting and sizing of mammalian cells in suspension. *Biophys. J*. 5:393–405. http://dx.doi.org/10.1016/S0006-3495(65)86724-8

Grover, W.H., A.K. Bryan, M. Diez-Silva, S. Suresh, J.M. Higgins, and S.R. Manalis. 2011. Measuring single-cell density. *Proc. Natl. Acad. Sci. USA*. 108:10992–10996. http://dx.doi.org/10.1073/pnas.1104651108

Habela, C.W., and H. Sontheimer. 2007. Cytoplasmic volume condensation is an integral part of mitosis. *Cell Cycle*. 6:1613–1620. http://dx.doi.org/10.4161/cc.6.13.4357

Huang, X., A.M. Dubuc, R. Hashizume, J. Berg, Y. He, J. Wang, C. Chiang, M.K. Cooper, P.A. Northcott, M.D. Taylor, et al. 2012. Voltage-gated potassium channel EAG2 controls mitotic entry and tumor growth in medulloblastoma via regulating cell volume dynamics. *Genes Dev*. 26:1780–1796. http://dx.doi.org/10.1101/gad.193789.112

Jiang, H., and S.X. Sun. 2013. Cellular pressure and volume regulation and implications for cell mechanics. *Biophys. J*. 105:609–619. http://dx.doi.org/10.1016/j.bpj.2013.06.021

Kondo, T., and S. Hayashi. 2013. Mitotic cell rounding accelerates epithelial invagination. *Nature*. 494:125–129. http://dx.doi.org/10.1038/nature11792

Lancaster, O.M., and B. Baum. 2014. Shaping up to divide: coordinating actin and microtubule cytoskeletal remodelling during mitosis. *Semin. Cell Dev. Biol*. 34:109–115. http://dx.doi.org/10.1016/j.semcdb.2014.02.015

Lancaster, O.M., M. Le Berre, A. Dimitracopoulos, D. Bonazzi, E. Zlotek-Zlotkiewicz, R. Picone, T. Duke, M. Piel, and B. Baum. 2013. Mitotic rounding alters cell geometry to ensure efficient bipolar spindle formation. *Dev. Cell.* 25:270–283. http://dx.doi.org/10.1016/j.devcel.2013.03.014

Le Berre, M., E. Zlotek-Zlotkiewicz, D. Bonazzi, F. Lautenschlaeger, and M. Piel. 2014. Methods for two-dimensional cell confinement. *Methods Cell Biol.* 121:213–229. http://dx.doi.org/10.1016/B978-0-12-800281-0.00014-2

Matthews, H.K., U. Delabre, J.L. Rohn, J. Guck, P. Kunda, and B. Baum. 2012. Changes in Ect2 localization couple actomyosin-dependent cell shape changes to mitotic progression. *Dev. Cell.* 23:371–383. http://dx.doi.org/10.1016/j.devcel.2012.06.003

Nakajima, Y., E.J. Meyer, A. Kroesen, S.A. McKinney, and M.C. Gibson. 2013. Epithelial junctions maintain tissue architecture by directing planar spindle orientation. *Nature.* 500:359–362. http://dx.doi.org/10.1038/nature12335

Ramanathan, S.P., J. Helenius, M.P. Stewart, C.J. Cattin, A.A. Hyman, and D.J. Muller. 2015. Cdk1-dependent mitotic enrichment of cortical myosin II promotes cell rounding against confinement. *Nat. Cell Biol.* 17:148–159. http://dx.doi.org/10.1038/ncb3098

Salbreux, G., G. Charras, and E. Paluch. 2012. Actin cortex mechanics and cellular morphogenesis. *Trends Cell Biol.* 22:536–545. http://dx.doi.org/10.1016/j.tcb.2012.07.001

Son, S., J. Ho Kang, S. Oh, M.W. Kirschner, T.J. Mitchison, and S.R. Manalis. 2015. Resonant microchannel volume and mass measurements show that suspended cells swell during mitosis. *J. Cell Biol.* http://dx.doi.org/10.1083/jcb.201505058

Stewart, M.P., J. Helenius, Y. Toyoda, S.P. Ramanathan, D.J. Muller, and A.A. Hyman. 2011. Hydrostatic pressure and the actomyosin cortex drive mitotic cell rounding. *Nature.* 469:226–230. http://dx.doi.org/10.1038/nature09642

Stylianopoulos, T., J.D. Martin, V.P. Chauhan, S.R. Jain, B. Diop-Frimpong, N. Bardeesy, B.L. Smith, C.R. Ferrone, F.J. Hornicek, Y. Boucher, et al. 2012. Causes, consequences, and remedies for growth-induced solid stress in murine and human tumors. *Proc. Natl. Acad. Sci. USA.* 109:15101–15108. http://dx.doi.org/10.1073/pnas.1213353109

Swift, J., I.L. Ivanovska, A. Buxboim, T. Harada, P.C. Dingal, J. Pinter, J.D. Pajerowski, K.R. Spinler, J.W. Shin, M. Tewari, et al. 2013. Nuclear lamin-A scales with tissue stiffness and enhances matrix-directed differentiation. *Science.* 341:1240104. http://dx.doi.org/10.1126/science.1240104

Tzur, A., R. Kafri, V.S. LeBleu, G. Lahav, and M.W. Kirschner. 2009. Cell growth and size homeostasis in proliferating animal cells. *Science.* 325:167–171. http://dx.doi.org/10.1126/science.1174294

Zangle, T.A., and M.A. Teitell. 2014. Live-cell mass profiling: an emerging approach in quantitative biophysics. *Nat. Methods.* 11:1221–1228. http://dx.doi.org/10.1038/nmeth.3175